Int. J. Electrochem. Sci., 13 **(2018)** 3843 – 3854, doi: 10.20964/2018.04.54

International Journal of
ELECTROCHEMICAL
SCIENCE
www.electrochemsci.org

Controlled Synthesis of Co_3O_4 Electrocatalysts with Different Morphologies and Their Application for Oxygen Evolution Reaction

Suxian Liu[1], *Rui Zhang*[2,*], *Weixin Lv*[2], *Fenying Kong*[2], *Wei Wang*[2,*]

[1] School of Chemistry and Chemical Engineering, Jiangsu University, Zhenjiang 212013, China
[2] School of Chemistry and Chemical Engineering, Yancheng Institute of Technology, Yancheng 224051, China
[*]E-mail: zhangrui20128@163.com, wangw@ycit.edu.cn

Received: 21 December 2017 / *Accepted:* 11 February 2018 / *Published:* 6 March 2018

The effect of the Co_3O_4 catalysts with different morphologies on the oxygen evolution reaction (OER) performance is not clearly. Herein, we have synthesized urchin-like Co_3O_4, Co_3O_4 nanosheets, Co_3O_4 nanoparticles and Co_3O_4 nanospheres. These Co_3O_4 materials with different morphologies are applied as the electrocatalysts for OER, and their OER performances are also compared with related literature results. The obtained overpotentials for OER are 308, 342, 350 and 448 mV at the current density of 10 mA cm^{-2} in 1 M KOH on urchin-like Co_3O_4, Co_3O_4 nanosheets, Co_3O_4 nanoparticles and Co_3O_4 nanospheres, respectively. The catalytic mechanism of the urchin-like Co_3O_4 for OER is explored by electrochemical oxidation of H_2O_2. This study is helpful to understand the relationship between the morphology and the OER performance of the Co_3O_4 electrocatalysts.

Keywords: Cobalt oxide; Oxygen evolution; Urchin-like; H_2O_2 sensor.

1. INTRODUCTION

In recent years, the environment pollution has become more and more serious, and the combustion of the fossil fuel is the main reason [1, 2]. Therefore, finding an efficient, clean and renewable energy is one of the difficult problems those must be solved as soon as possible. Electrocatalytic water splitting provides a sustainable strategy to supply clean hydrogen energy through hydrogen evolution reaction (HER) and oxygen evolution reaction (OER) [3]. For water electrolysis, the energy loss at the anode is significant, because OER is a thermodynamic uphill reaction involving a stepwise four electron transfer at a high overpotential [4, 5].

Thus far, it still remains a great challenge to develop efficient OER catalysts which can help to reduce the overpotential for OER. Several noble metal catalysts, such as RuO_2, IrO_2 and their combinations with other metals, are still considered as the most active catalysts for OER [6, 7]. However, these noble metal catalysts are not economical due to the high cost and element scarcity. Therefore, great efforts have been undertaken to develop cheap and efficient materials for catalyzing OER to replace the expensive noble metal catalysts [8, 9]. Co_3O_4 based catalyst is considered to be a promising electroactive material due to its low cost, environmental friendliness and high catalytic performance [10]. At present, a lot of Co_3O_4 materials with different morphologies, such as nanoparticles [11, 12], nanorods [13, 14], nanowires [15, 16], nanosheets [17, 18] or porous structures [19, 20], have been studied as the OER catalysts. It is difficult to understand the effect of the morphology of Co_3O_4 on the OER performance by comparing different literature, because some systemic factors (the catalyst loading, the substrate materials, the distance between the electrodes or the concentration of the Nafion solution, etc.) may affect the experimental results. Therefore, the effect of the Co_3O_4 catalysts with different morphologies on the OER performance is not clearly and need to be further studied.

Herein, we synthesized urchin-like Co_3O_4, Co_3O_4 nanosheets, Co_3O_4 nanoparticles and Co_3O_4 nanospheres. These Co_3O_4 materials with different morphologies were applied as the electrocatalysts for OER, and their OER performances were also compared with related literature results. The catalytic mechanism of the urchin-like Co_3O_4 for OER was explored by electrochemical measurements.

2. EXPERIMENTAL

2.1 Synthesis of urchin-like Co_3O_4

9.7 g of cobalt nitrate hexahydrate ($Co(NO_3)_2{\cdot}6H_2O$) and 0.5 g of urea were dissolved in deionized water (35 mL) under vigorous stirring for 1 h. Then, the mixed solution was transferred into a 50 mL Teflon-lined autoclave, sealed, and maintained at 160 °C for 12 h. After cooling to room temperature, the obtained precipitates were centrifuged, washed with deionized water and ethanol many times. Finally, the as-prepared red powders were calcined in a muffle furnace at 300 °C for 1 h in static air to obtain urchin-like Co_3O_4 labeled as Co_3O_4-1.

2.2 Synthesis of Co_3O_4 nanosheets and nanoparticles

0.969 g of $Co(NO_3)_2{\cdot}6H_2O$ and 1 g of urea were dissolved in deionized water (40 mL) under vigorous stirring for 1 h. Then, the mixed solution was transferred into a 50 mL autoclave, sealed, and maintained at 160 °C for 6 h. After cooling to room temperature, the precipitates were centrifuged, washed with deionized water and ethanol many times. Finally, the as-prepared powders were calcined in a muffle furnace at 300 °C for 2 h in static air to obtain Co_3O_4 nanosheets labeled as Co_3O_4-2. For obtaining the Co_3O_4 nanoparticles, the preparation process was similar to that of Co_3O_4 nanosheets, only in the first step, 40 mL of deionized water was replaced by 40 mL of ethanol. The as-prepared

Co_3O_4 nanoparticles were labeled as Co_3O_4-3.

2.3 Synthesis of Co_3O_4 nanospheres

58.21 g of $Co(NO_3)_2 \cdot 6H_2O$ and 2 g of sodium hydroxide were dissolved in deionized water (40 mL) under vigorous stirring for 10 min. Then the purple mixed solution was transferred into a 50 mL autoclave, sealed, and maintained at 180 °C for 5 h. After cooling to room temperature, the precipitates were centrifuged, washed with deionized water and ethanol for many times, and dried in vacuum at 60 °C for 10 h. Finally, the as-prepared powders were calcined in a muffle furnace at 500 °C for 3 h in static air to obtain Co_3O_4 nanospheres labeled as Co_3O_4-4.

2.4 Materials characterization

The crystal structures of the samples were characterized via X-ray diffraction (XRD, Bluker Rigaku D/MAX 2200 diffractometer with Cu Kα). The morphologies of the samples were investigated via field emission scanning electron microscopy (FE-SEM, Nova NanoSEM 450). X-ray photoelectron spectroscopy (XPS) measurements were performed using a VG ESCALAB 250 electron spectrometer.

2.5 Electrochemical measurements

All the electrochemical measurements were performed in a standard three-electrode system with a CHI 660E electrochemical workstation using 1 M KOH aqueous solution as an electrolyte. A Pt plate (2 cm^2) and a Hg/HgO electrode (in 1 M KOH solution) were used as the counter and reference electrodes, respectively. In this work, all of the potentials were calibrated to a reversible hydrogen electrode (RHE) according to $E(\text{RHE}) = E(\text{Hg/HgO}) + 0.059 \times \text{pH} + 0.098$ V. The working electrode was a L-style glassy carbon electrode coated with the as-prepared Co_3O_4 catalysts. The working electrode was prepared as follows: 3 mg of catalyst and 6 μL of Nafion solution (5 wt%) were dispersed in 200 μL ethanol by sonicating for 1 h to form a homogeneous ink. Then 5 μL of the catalyst ink was coated on the L-style glassy carbon electrode with a diameter of 3 mm (loading 1 mg cm^{-2}).

Before measuring, each working electrode was cycled 20 times by cyclic voltammetry (CV) at a scan rate of 100 mV s^{-1}. Linear sweep voltammetry (LSV) was performed at a scan rate of 5 mV s^{-1}. The durability tests for OER were performed at 1.54 V. The LSV curves were recorded before and after the durability tests. Electrochemical impedance spectroscopy (EIS) was performed at 1.62 V in a frequency range from 10^5 to 0.1 Hz by applying an AC voltage with 5 mV amplitude. Every electrochemical experiment was performed three times and exhibited excellent reproducibility. The overpotential (η) was calculated through $\eta = E(\text{RHE}) - 1.23$ V. To evaluate the electrochemical activity of the Co_3O_4-1 catalyst towards H_2O_2 oxidation, H_2O_2 (30 vol%) solution was used for electrochemical measurement.

3. RESULTS AND DISCUSSION

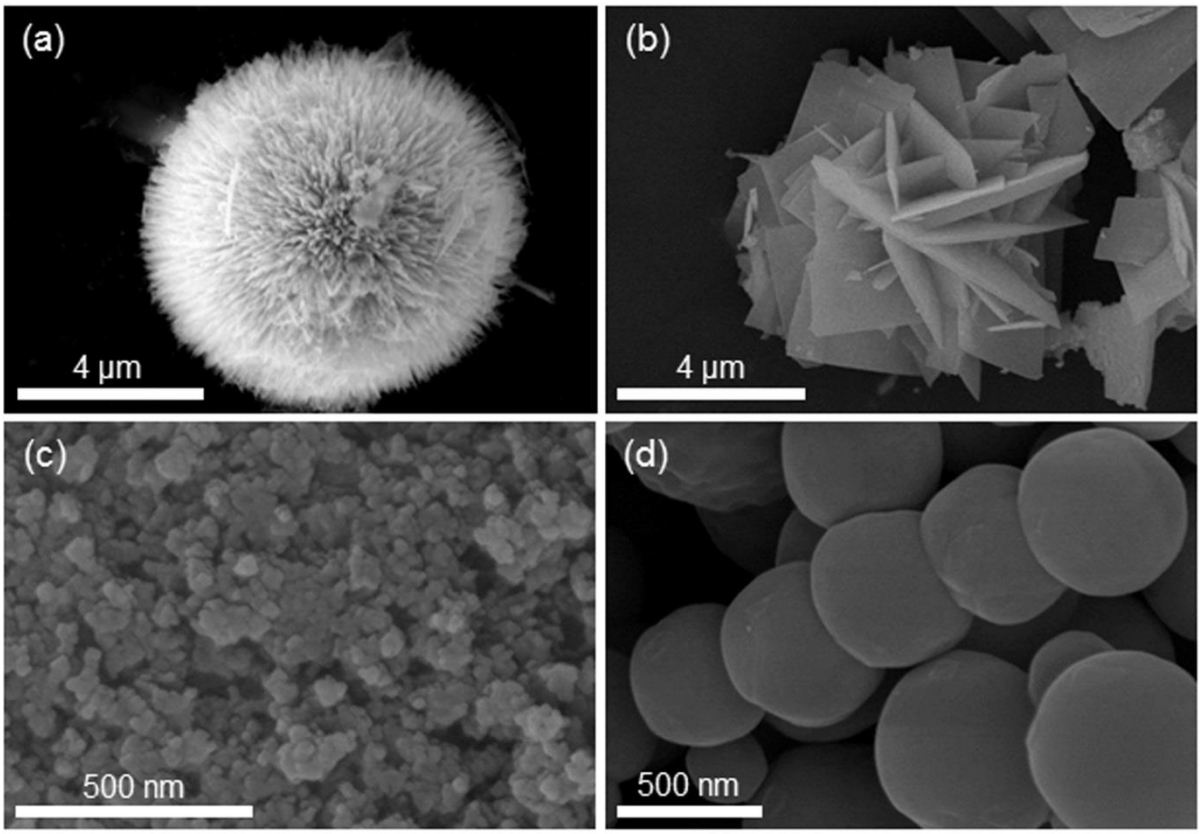

Figure 1. SEM images of (a) Co_3O_4-1, (b) Co_3O_4-2, (c) Co_3O_4-3, and (d) Co_3O_4-4.

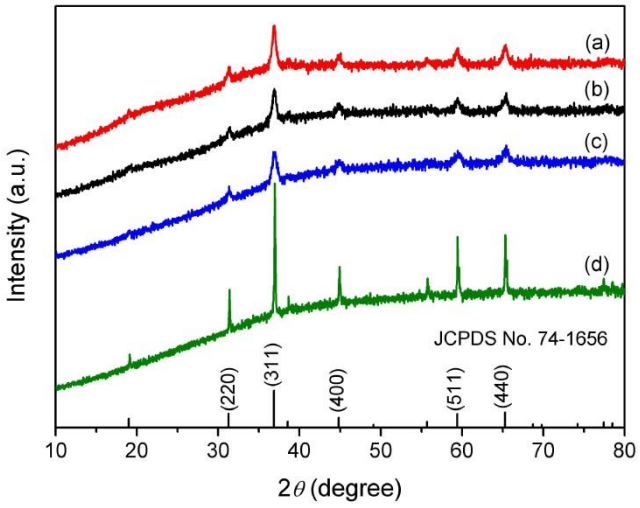

Figure 2. XRD patterns of (a) Co_3O_4-1, (b) Co_3O_4-2, (c) Co_3O_4-3, and (d) Co_3O_4-4.

Fig. 1 shows four kinds of morphologies of the as-prepared Co_3O_4 samples. As shown in Fig. 1a, the Co_3O_4-1 has the three-dimensional nanostructure of urchin-like spheres with the diameter of about 10 μm and are composed of lots of nanowires gathered as a ring in the center, which may give it a large specific surface area. Co_3O_4-2 has the structure of nanosheets with the thickness of around 90

nm (Fig. 1b). We can clearly see from Figs. 1c and 1d that Co_3O_4-3 with the nanoparticles structure and Co_3O_4-4 with the nanospheres structure have an approximate average diameter of 28 and 570 nm, respectively.

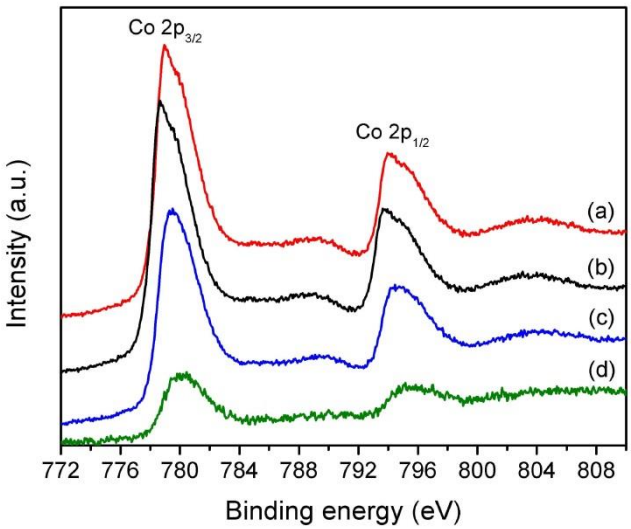

Figure 3. XPS spectra of the Co 2p region recorded with (a) Co_3O_4-1, (b) Co_3O_4-2, (c) Co_3O_4-3, and (d) Co_3O_4-4.

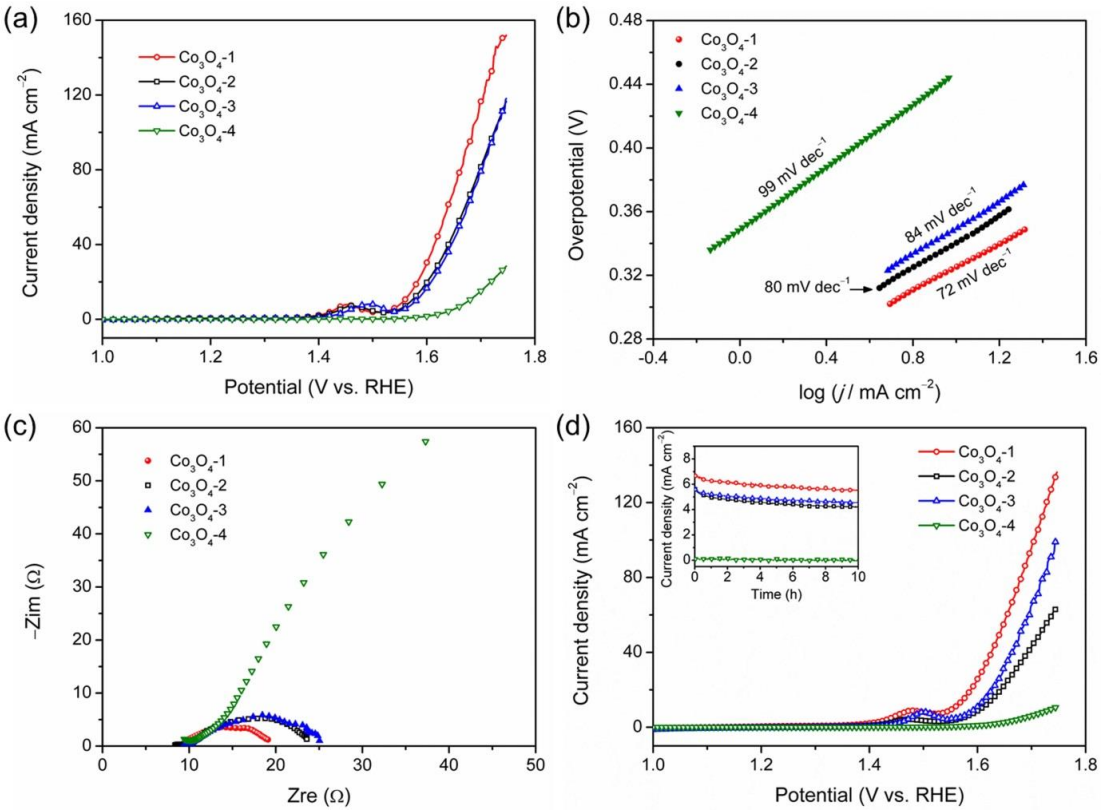

Figure 4. (a) LSV curves, and (b) Tafel plots of four kinds of Co_3O_4 catalysts recorded in 1 M KOH; (c) Nyquist plots of four kinds of Co_3O_4 catalysts recorded at 1.62 V; (d) LSV curves of four kinds of Co_3O_4 catalysts recorded in 1 M KOH after stability test, the inset of Fig. 4d is the stability tests of four kinds of Co_3O_4 catalysts for 10 h in 1 M KOH at 1.54 V.

To identify the crystal structures of the as-prepared Co_3O_4 samples, the XRD patterns were collected and are shown in Fig. 2. All of the diffraction peaks can be perfectly indexed and assigned to the cubic phase of Co_3O_4 (JCPDS PDF No. 74-1656). No other peaks could be observed from the patterns. It can be seen that the crystallinity of Co_3O_4-4 is higher than those of other samples. But it was reported that the weak crystallinity of the material may lead to abundant exposed active sites [21]. The XPS spectra of different Co_3O_4 samples in the Co 2p region are shown in Fig. 3. Two major peaks (Co $2p_{3/2}$ and Co $2p_{1/2}$) are observed with a spin energy separation of ca. 15.4 eV, which corresponds to a typical Co_3O_4 phase with both Co^{2+} and Co^{3+} cations [22, 23].

OER activities of four kinds of Co_3O_4 catalysts are investigated through LSV in 1 M KOH. As shown in Fig. 4a, the Co_3O_4-1 catalyst presents the lowest onset potential of 1.51 V among the four catalysts. In order to obtain an exchange current density of 10 mA cm^{-2}, the overpotentials of 308, 342, 350 and 448 mV are needed for the Co_3O_4-1, Co_3O_4-2, Co_3O_4-3 and Co_3O_4-4 catalysts, respectively. Tafel plots for OER activity on the as-prepared Co_3O_4 catalysts are presented in Fig. 4b. The Tafel slope of Co_3O_4-1 is calculated as 72 mV dec^{-1}, which is smaller than those of Co_3O_4-2 (80 mV dec^{-1}), Co_3O_4-3 (84 mV dec^{-1}) and Co_3O_4-4 (99 mV dec^{-1}). Both the low overpotential and small Tafel slope of the Co_3O_4-1 catalyst implies the favorable catalytic activity for OER on Co_3O_4-1. The good catalytic activity of Co_3O_4-1 for OER can be ascribed to the unique urchin-like nanostructure, because this nanostructure may prevent the oxygen bubbles accumulating and the oxygen bubbles may quick remove from the electrode surface [24].

OER occurs through a complex four-electron transfer process. The proposed OER mechanism is the following two pathways: (1) OH^{ads} generated from OH^- (or H_2O) is oxidized to O_2^{ads} directly through a one-step process; (2) the OH^{ads} is oxidized to peroxo species (OOH^{ads}) firstly, and then the OOH^{ads} is oxidized to O_2^{ads} in a two-step process [25]. As we known, the Tafel slope value could preliminary determine the reaction mechanism according to the calculated electron transfer number. In this work, the Tafel slopes of the Co_3O_4 catalysts toward OER are much bigger than 30 mV dec^{-1} which is the ideal Tafel slope value of the four-electron pathway [21]. To verify the OER pathway of Co_3O_4-1, the electron transfer number of OER on Co_3O_4-1 was calculated based on the obtained Tafel slope value. The following equation is the Bulter-Volmer equation:

$$\beta_A = \frac{2.303 \times R \times T}{\alpha_A \times n \times F} \quad (1)$$

where β_A is the Tafel slope, R is the universal gas constant, T is the reaction temperature, α_A is the symmetric factor (typical being in the range of 0.4 to 0.6), n is the number of exchanged electrons in the reaction, and F is the Faraday constant. Herein, if α_A is 0.5, n is about 1.64 (close to 2), indicating that the OER on Co_3O_4-1 coincides with the two-step process, and OOH^{ads} is the intermediate. The possible OER mechanism of Co_3O_4-1 proceeds via a two-step process as follows [26]:

$M–OH_2 + OH^- \rightarrow M–OH + H_2O + e^-$

$M–OH + OH^- \rightarrow M–O^* + H_2O + e^-$

$M–O^* + OH^- \rightarrow M–OOH + e^-$

$M–OOH + OH^- \rightarrow M–OH_2 + O_2 + e^-$

In the Nyquist plots of four kinds of Co_3O_4 catalysts (Fig. 4c), Co_3O_4-1 has small semicircle diameter compared to other Co_3O_4 catalysts, which indicates that the excellent OER activity of Co_3O_4-1 is partially attributed to its efficient charge transfer efficiency. The durability of the Co_3O_4 catalysts for electrocatalytic OER in 1 M KOH solution was evaluated with chronoamperometry tests. As shown in the inset of Fig. 4d, during the 10 h of stability test at 1.54 V, the Co_3O_4-4 catalyst has no activity, and the activities of other Co_3O_4 catalysts decrease. After 10 h of stability tests, LSV measurements were performed and the results are shown in Fig. 4d. It can be seen that Co_3O_4-1 still exhibits excellent OER activity. At the current density of 10 mA cm^{-2}, Co_3O_4-1 has an overpotential of 324 mV, which is still lower than Co_3O_4-2 (377 mV), Co_3O_4-3 (366 mV) and Co_3O_4-4 (509 mV). By comparing the LSV curves in Figs. 4a and 4d, it can be found that the OER performances of Co_3O_4 catalysts show small decrease after the stability tests.

It is very important to compare the OER performance of the catalysts with the related literature results. Table 1 shows the overpotentials and Tafel slopes of the catalysts for OER in 1 M KOH. It can be seen that Co_3O_4-1 catalyst in this work is not inferior to other reported highly efficient OER catalysts.

Table 1. Comparison of the electrocatalytic performances of Co_3O_4 catalysts and the related materials reported in literature at the current density of 10 mA cm^{-2} in 1 M KOH for OER.

Catalyst	Overpotential (mV)	Tafel slope (mV dec^{-1})	Reference
Urchin-like sphere arrays Co_3O_4	~270	65	[8]
Co_3O_4 quantum dots	270	39	[10]
Oxygen deficient Co_3O_4 nanorods	275	-	[13]
Mesoporous Co_3O_4 nanowires	~405	72	[16]
Co_3O_4 mesoporous nanostructures	360	89	[20]
rGO-Co_3O_4 yolk-shell nanocage	410	85	[22]
Co_3O_4/$NiCo_2O_4$ double-shelled nanocages	340	88	[27]
Mesoporous Co_3O_4 nanoflakes	380	48	[28]
Mesoporous Co_3O_4	390	74	[29]
Porous Co_3O_4 nanosheets	368	59	[30]
Co_3O_4 nanocubes/graphene	402	67	[31]
Co_3O_4-C nanowire arrays/Ni foam	310	90	[32]
Co_3O_4 nanocubes/N-doped graphene	280	69	[33]
CoP hollow polyhedron	400	57	[34]
Coral-like CoSe	295	40	[35]
Co_3O_4-1	308	72	This work
Co_3O_4-2	342	80	This work
Co_3O_4-3	350	84	This work
Co_3O_4-4	448	99	This work

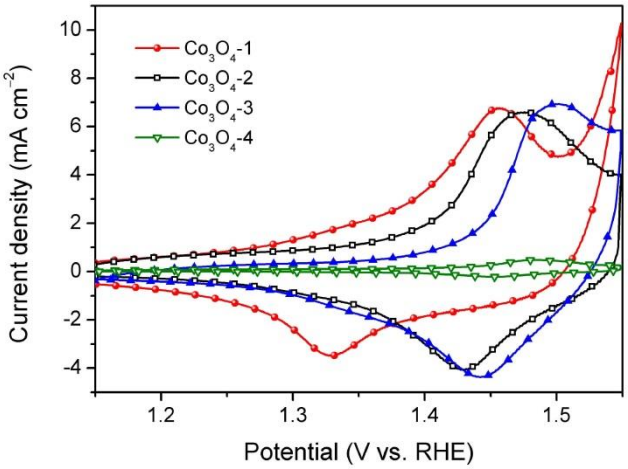

Figure 5. CV curves of four kinds of Co_3O_4 catalysts at the scan rate of 5 mV s^{-1}.

In Fig. 4a, there is a peak before the OER occurs. As shown in the CV curves at the corresponding potential range (Fig. 5), a pair of redox peaks for Co_3O_4 at 1.47 V (anodic) and 1.37 V (cathodic) is observable for the four kinds of Co_3O_4 catalysts. It was reported that the oxidation of Co^{3+} to Co^{4+} is crucial for OER activity [29, 36]. At the corresponding potential range, there is not only one redox couple of Co^{III}/Co^{IV}, but also another redox couple of Co^{II}/Co^{III} [29, 37]. But only one redox couple can be seen clearly in Fig. 5.

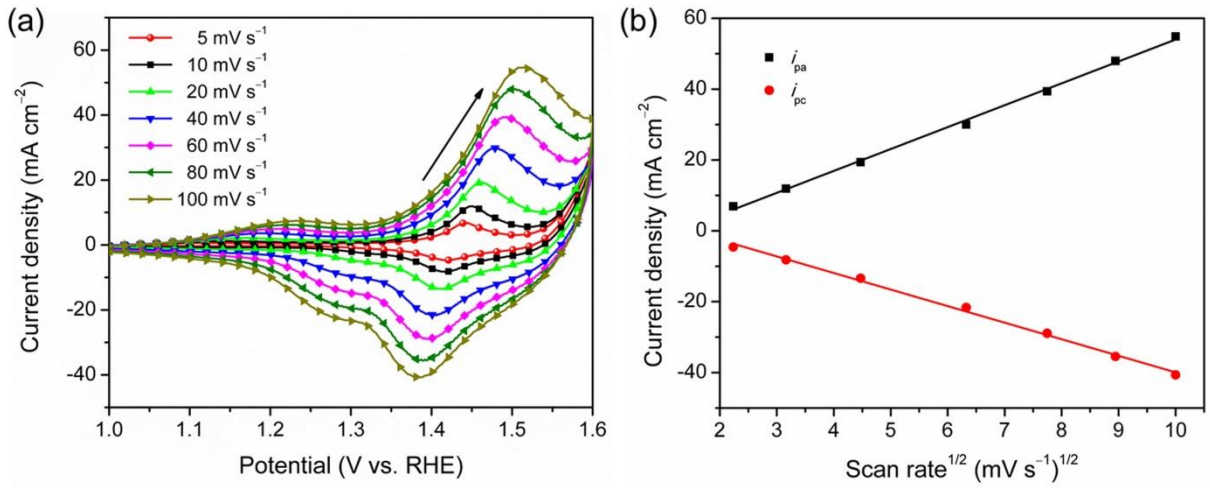

Figure 6. (a) CV curves of Co_3O_4-1 in 1 M KOH measured at different scan rates (5~100 mV s^{-1}); (b) linear calibration relationship between the anodic and cathodic peak current densities and the square root of the scan rate.

CV curves of Co_3O_4-1 in 1 M KOH at different scan rates are shown in Fig. 6a. Two redox couple can be seen when the scan rate increases. The obvious pair of redox peaks, the anodic peak at around 1.45 V and the cathodic peak at around 1.4 V, are also associated to the electrochemical

transformation of Co^{III}/Co^{IV} (1.2 and 1.15 V are attribute to Co^{II}/Co^{III}). The cathodic peak current density (i_{pc}) and anodic peak current density (i_{pa}) increase as the increase of the scan rate. Apparently, the relationship between the peak current densities of Co^{III}/Co^{IV} and the square root of the scan rate ($\nu^{1/2}$) can be evaluated by the series linear plots (Fig. 6b). The calibration plots can be described by equations (2) and (3):

$$i_{pa} = 6.18\ \nu^{1/2} - 4.67 \quad (R^2 = 0.997) \qquad (2)$$

$$i_{pc} = -4.67\ \nu^{1/2} + 6.80 \quad (R^2 = 0.996) \qquad (3)$$

According to the characteristic indexes of the heterogeneous electron transfer reaction, the electron transfer kinetics of the Co^{III}/Co^{IV} couple is controlled by diffusion confinement. It indicates that the peaks in Fig. 4a can be assigned to the formation of Co^{IV} from Co^{III} that is easy to happen.

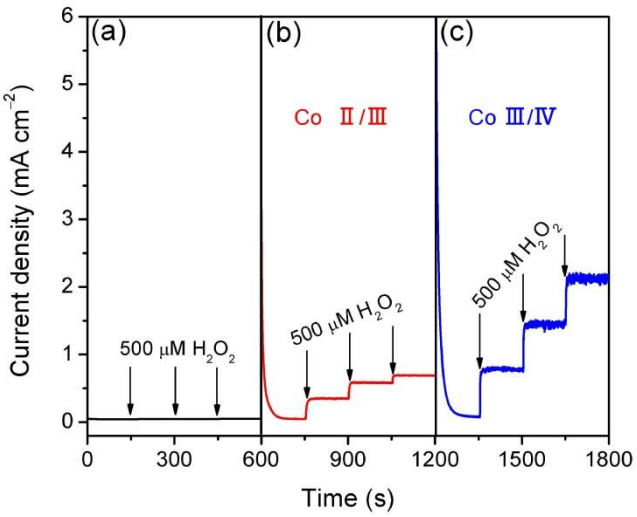

Figure 7. *I-t* curves of Co_3O_4-1 for the addition of 500 μM H_2O_2 in 1 M KOH each time when the potential is holding at 1 V (a), 1.22 V (b), and 1.45 V (c).

It was reported that Co^{IV} cations are required to catalyze OER [15], but its mechanism is not clearly. Yeo et al. found that the peroxo species (OOH^{ads}) and Co^{IV} as catalytic active sites actually emerge in the activated catalysts during the OER process through combining with in situ spectrum techniques [36]. The Tafel results in this work showed that the electron transfer pathway of Co_3O_4-1 is the two-step process, in which the peroxo species (OOH^{ads}) is the intermediate. It is noteworthy that Co^{III}/Co^{IV} redox couple happens to be the catalyst for H_2O_2 oxidation [38]. Therefore, the electrocatalytic oxidation of H_2O_2 on Co_3O_4-1 was further studied due to the easy transformation from H_2O_2 to OOH^{ads}. As shown in Fig. 7, when the potential is holding at 1 V which is far below the potential of Co^{III}/Co^{IV} couple, no obvious current can be observed. The oxidation current density of 500 μM H_2O_2 increases as the activated potential increases from 1.22 to 1.45 V, which indicates that the Co^{III}/Co^{IV} redox couple formed at around 1.45 V can actually facilitate the oxidation of OOH^{ads}. To further evaluate the catalytic activity of the Co_3O_4-1 towards H_2O_2 oxidation, the typical amperometric response of Co_3O_4 to the successive addition of different amounts of H_2O_2 into the stirring 1 M KOH is recorded at 1.45 V. As the concentration of H_2O_2 increases, the electrochemical response of Co_3O_4-1

displays a typical staircase curve in Fig. 8a. The Co_3O_4 activity in the reaction with H_2O_2 can be described by the calibration curve in Fig. 8b. The increase of the current density is proportional to the H_2O_2 concentration, and the linear response for H_2O_2 is expressed as: I (μA) = 1.18 (μA $μM^{-1}$) c (μM, H_2O_2) + 68 (μA) (R^2 = 0.997). Derived from the calibration curve, the electrochemical response of Co_3O_4 towards H_2O_2 can reach as low as 17.5 μM (S/N = 3). The results suggest that Co^{III}/Co^{IV} redox couple formed at 1.45 V can oxide H_2O_2 at low concentration. It indicates that the fourth electron transfer step of OER is a fast kinetics process.

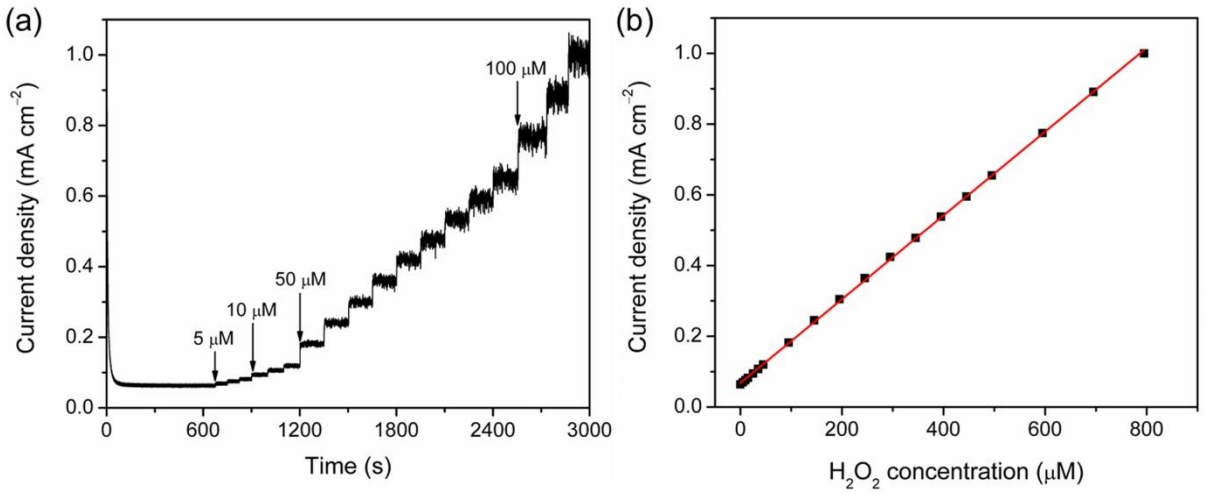

Figure 8. *I-t* curve of Co_3O_4-1 (holding at 1.45 V) for the successive addition of H_2O_2 in 1 M KOH; (b) linear calibration relationship of current densities vs. H_2O_2 concentration.

As shown in Fig. 7, the current density at 1.45 V is as small as that at 1 V before H_2O_2 is not added. It indicates that the third step (OH oxidation to OOH^{ads}) does not happen at the potential of 1.45 V. If the third step happens, the generated OOH^{ads} can be rapidly oxidized to O_2^{ads} by the nearby Co^{III}/Co^{IV} redox couple. It is obviously that the strong oxidation ability of the Co^{III}/Co^{IV} redox couple for OOH^{ads} could facilitate the formation of O_2^{ads}. The OER mechanism is complex, many factors may affect the electron transfer pathway, including the formation/decomposition of unstable intermediate-oxides on the surface of catalysts, the recombination of oxygen atoms, the desorption/adsorption processes, the chemical reactions and the electroconductivity of the catalysts. More works should be carried out for understanding the OER mechanism.

4. CONCLUSIONS

In summary, urchin-like Co_3O_4, Co_3O_4 nanosheets, Co_3O_4 nanoparticles, and Co_3O_4 nanospheres were successfully synthesized. Among the four kinds of Co_3O_4 catalysts with different morphologies, the urchin-like Co_3O_4 shows the best OER catalytic performance. The urchin-like Co_3O_4 exhibits a low overpotential of 308 mV at the current density of 10 mA cm^{-2}, and a small Tafel slope of 72 mV dec^{-1}. The Tafel results in this work showed that the electron transfer pathway of

Co_3O_4-1 is a two-step process, in which the peroxo species (OOH^{ads}) is the intermediate. The urchin-like Co_3O_4 shows excellent electrooxidation performance towards H_2O_2 when Co^{IV} cations formed (at 1.45 V vs. RHE) which indicates that the fourth electron transfer step of OER is a fast kinetics process on Co_3O_4 catalysts.

ACKNOWLEDGEMENTS
The work was supported by the National Natural Science Foundation of China (21603184, 21675139, 21575123); and the joint research fund between Collaborative Innovation Center for Ecological Building Materials and Environmental Protection Equipments and Key Laboratory for Advanced Technology in Environmental Protection of Jiangsu Province.

References

1. W. X. Lv, J. Zhou, J. J. Bei, R. Zhang, L. Wang, Q. Xu and W. Wang, *Appl. Surf. Sci.*, 393 (2017) 191.
2. W. X. Lv, J. J. Bei, R. Zhang, W. J. Wang, F. Y. Kong, L. Wang and W. Wang, *ACS Omega*, 2 (2017) 2561.
3. M. Leng, X. L. Huang, W. Xiao, J. Ding, B. H. Liu, Y. H. Du and J. M. Xue, *Nano Energy*, 33 (2017) 445.
4. Q. Zhao, Z. Yan, C. Chen and J. Chen, *Chem. Rev.*, 117 (2017) 10121.
5. W. X. Lv, S. X. Liu, R. Zhang, W. J. Wang, Z. X. Wang, L. Wang and W. Wang, *J. Mater. Sci.*, 53 (2018) 4939.
6. T. Audichon, S. Morisset, T. W. Napporn, K. B. Kokoh, C. Comminges and C. Morais, *Chemelectrochem*, 2 (2015) 1128.
7. Z. S. Song, X. P. Han, Y. D. Deng, N. Q. Zhao, W. B. Hu and C. Zhong, *ACS Appl. Mater. Inter.*, 9 (2017) 22694.
8. R. C. Li, D. Zhou, J. X. Luo, W. M. Xu, J. W. Li, S. S. Li, P. P. Cheng and D. S. Yuan, *J. Power Sources*, 341 (2017) 250.
9. W. Zhang, W. Z. Lai and R. Cao, *Chem. Rev.*, 117 (2017) 3717.
10. G. X. Zhang, J. Yang, H. Wang, H. B. Chen, J. L. Yang and F. Pan, *ACS Appl. Mater. Inter.*, 9 (2017) 16159.
11. Y. R. Liu, G. Q. Han, X. Li, B. Dong, X. Shang, W. H. Hu, Y. M. Chai, Y. Q. Liu and C. G. Liu, *Int. J. Hydrogen Energ.*, 41 (2016) 12976.
12. J. D. Blakemore, H. B. Gray, J. R. Winkler and A. M. Mueller, *ACS Catal.*, 3 (2013) 2497.
13. G. Cheng, T. Kou, J. Zhang, C. Si, H. Gao and Z. Zhang, *Nano Energy*, 38 (2017) 155.
14. Y. X. Zhang, X. Guo, X. Zhai, Y. M. Yan and K. N. Sun, *J. Mater. Chem. A*, 3 (2015) 1761.
15. S. Xu, J. L. Tong, Y. Liu, W. Hu, G. B. Zhang and Q. H. Xia, *J. Renew. Sustain. Ener.*, 8 (2016) 044703.
16. Y. Wang, T. Zhou, K. Jiang, P. Da, Z. Peng, J. Tang, B. Kong, W. B. Cai, Z. Yang and G. Zheng, *Adv. Energy Mater.*, 4 (2014) 1400696.
17. L. Xu, Q. Q. Jiang, Z. H. Xiao, X. Y. Li, J. Huo, S. Y. Wang and L. M. Dai, *Angew. Chem. Int. Ed.*, 55 (2016) 5277.
18. X. L. Zhang, J. B. Zhang and K. Wang, *ACS Appl. Mater. Inter.*, 7 (2015) 21745.
19. H. Tueysuez, Y. J. Hwang, S. B. Khan, A. M. Asiri and P. Yang, *Nano Res.*, 6 (2013) 47.
20. H. Sun, Y. Zhao, K. Molhave, M. Zhang and J. Zhang, *Nanoscale*, 9 (2017) 14431.
21. S. C. Du, Z. Y. Ren, Y. Qu, J. Wu, W. Xi, J. Q. Zhu and H. G. Fu, *Chem. Commun.*, 52 (2016) 6705.
22. Z. L. Wu, L. P. Sun, M. Yang, L. H. Huo, H. Zhao and J. C. Grenier, *J. Mater. Chem. A*, 4 (2016)

13534.
23. B. C. He, X. X. Chen, J. M. Lu, S. D. Yao, J. Wei, Q. Zhao, D. S. Jing, X. N. Huang and T. Wang, *Electroanal.*, 28 (2016) 2435.
24. J. H. Zhang, J. Y. Feng, T. Zhu, Z. L. Liu, Q. Y. Li, S. Z. Chen and C. W. Xu, *Electrochim. Acta*, 196 (2016) 661.
25. I. Katsounaros, S. Cherevko, A. R. Zeradjanin and K. J. J. Mayrhofer, *Angew. Chem. Int. Ed.*, 53 (2014) 102.
26. H. Y. Wang, S. F. Hung, H. Y. Chen, T. S. Chan, H. M. Chen and B. Liu, *J. Am. Chem. Soc.*, 138 (2016) 36.
27. H. Hu, B. Guan, B. Xia and X. W. Lou, *J. Am. Chem. Soc.*, 137 (2015) 5590.
28. S. Q. Chen, Y. F. Zhao, B. Sun, Z. M. Ao, X. Q. Xie, Y. Y. Wei and G. X. Wang, *ACS Appl. Mater. Inter.*, 7 (2015) 3306.
29. W. Song, Z. Ren, S. Y. Chen, Y. Meng, S. Biswas, P. Nandi, H. A. Elsen, P. X. Gao and S. L. Suib, *ACS Appl. Mater. Inter.*, 8 (2016) 20802.
30. Z. P. Li, X. Y. Yu and U. Paik, *J. Power Sources*, 310 (2016) 41.
31. P. Zhang, X. T. Han, H. Hu, J. Z. Gui, M. Y. Li and J. S. Qiu, *Catal. Commun.*, 88 (2017) 81.
32. J. T. Ren, G. G. Yuan, C. C. Weng and Z. Y. Yuan, *ACS Sustain. Chem. Eng.*, 6 (2018) 707.
33. S. K. Singh, V. M. Dhavale and S. Kurungot, *ACS Appl. Mater. Inter.*, 7 (2015) 442.
34. M. J. Liu and J. H. Li, *ACS Appl. Mater. Inter.*, 8 (2016) 2158.
35. M. Liao, G. F. Zeng, T. T. Luo, Z. Y. Jin, Y. J. Wang, X. M. Kou and D. Xiao, *Electrochim. Acta*, 194 (2016) 59.
36. B. S. Yeo and A. T. Bell, *J. Am. Chem. Soc.*, 133 (2011) 5587.
37. A. Bergmann, E. Martinez-Moreno, D. Teschner, P. Chernev, M. Gliech, J. F. de Araujo, T. Reier, H. Dau and P. Strasser, *Nature Commun.*, 6 (2015) 8625.
38. S. Barkaoui, M. Haddaoui, H. Dhaouadi, N. Raouafi and F. Touati, *J. Solid State Chem.*, 228 (2015) 226.